

See discussions, stats, and author profiles for this publication at: <https://www.researchgate.net/publication/279808101>

# Toward Accumulation of Magnetic Nanoparticles into Tissues of Small Porosity

ARTICLE *in* LANGMUIR · JULY 2015

Impact Factor: 4.46 · DOI: 10.1021/acs.langmuir.5b01458 · Source: PubMed

---

READS

65

## 6 AUTHORS, INCLUDING:



Rasam Soheilianx

Northeastern University

3 PUBLICATIONS 9 CITATIONS

[SEE PROFILE](#)



Allan E David

Auburn University

49 PUBLICATIONS 1,395 CITATIONS

[SEE PROFILE](#)



Hamed Abdi

Northeastern University

2 PUBLICATIONS 1 CITATION

[SEE PROFILE](#)



Randall M Erb

Northeastern University

39 PUBLICATIONS 779 CITATIONS

[SEE PROFILE](#)

## Toward Accumulation of Magnetic Nanoparticles into Tissues of Small Porosity

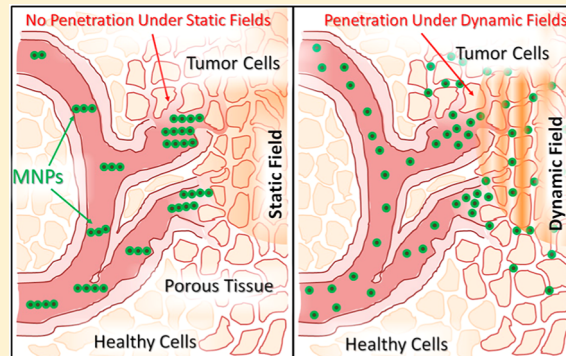
Rasam Soheilian,<sup>†</sup> Young Suk Choi,<sup>‡</sup> Allan E. David,<sup>‡</sup> Hamed Abdi,<sup>†</sup> Craig E. Maloney,<sup>†</sup> and Randall M. Erb\*,<sup>†</sup>

<sup>†</sup>Department of Mechanical and Industrial Engineering, Northeastern University, Boston, Massachusetts 02115, United States

<sup>‡</sup>Department of Chemical Engineering, Auburn University, Auburn, Alabama 36849, United States

### Supporting Information

**ABSTRACT:** Magnetic concentration of drug-laden magnetic nanoparticles has been proven to increase the delivery efficiency of treatment by 2-fold. In these techniques, particles are concentrated by the presence of a magnetic source that delivers a very high magnetic field and a strong magnetic field gradient. We have found that such magnetic conditions cause even 150 nm particles to aggregate significantly into assemblies that exceed several micrometers in length within minutes. Such assembly sizes exceed the effective intercellular pore size of tumor tissues preventing these drug-laden magnetic nanoparticles from reaching their target sites. We demonstrate that by using dynamic magnetic fields instead, we can break up these magnetic nanoparticles while simultaneously concentrating them at target sites. The dynamic fields we investigate involve precessing the field direction while maintaining a field gradient. Manipulating the field direction drives the particles into attractive and repulsive configurations that can be tuned to assemble or disassemble these particle clusters. Here, we develop a simple analytic model to describe the kinetic thresholds of disassembly and we compare both experimental and numerical results of magnetic particle suspensions subjected to dynamic fields. Finally we apply these methods to demonstrate penetration in a porous scaffold with a similar pore size to that expected of a tumor tissue.



### INTRODUCTION

Despite decades of effort developing more effective diagnostic and therapeutic tools, cancer remains the cause of almost 30% of all deaths each year.<sup>1</sup> While traditional chemotherapies have shown some efficacy against cancer, their broad distribution throughout the body and associated toxic side effects limit dosing to subtherapeutic concentrations of drug in the cancer (neoplastic) tissue.<sup>2</sup> Recent developments in nanomedicine with receptor targeting and further understanding of the leaky vasculature properties of tumors has significantly improved targeting. Still, the percent of injected dose (% ID/(g of tissue)) that distributes into the tumor is generally below 10%.<sup>3,4</sup> It has been shown that magnetic targeting could be applied with magnetic nanoparticles (MNPs) to greatly improve delivery of drugs to tumors.<sup>5</sup> These methods, however, have so far used simple static magnetic fields and gradients to concentrate the MNPs at the tumor site. Under these static fields, magnetic particles, even those as small as 150 nm in diameter, have been observed to agglomerate after only a few minutes.<sup>6</sup> This agglomeration hinders the extravasation of nanoparticles from the tumor vessels, which have pore cutoff sizes less than 600–800 nm,<sup>7,8</sup> and would greatly limit their mobility deep into a tumor tissue.

In other contexts, the breakup of magnetically chained particles and droplets under simple rotating magnetic fields has

been heavily investigated<sup>9–16</sup> and may be utilized to both concentrate the drug-laden magnetic nanoparticles within a tumor and enable extravasation through the leaky vasculature by preventing particle aggregation. For example, the effects of rotating magnetic fields on chain growth in magnetic particle suspensions were previously addressed, and it has been reported that the chain length decreases as the rotational frequency is increased.<sup>10</sup> Rotational dynamics of cross-linked chains have also been studied in order to do microscale mixing.<sup>9,11,12</sup> As we find in this work, however, MNP aggregation occurs rapidly, even in the presence of Brownian motion, and the average aggregate size quickly surpasses the typical pore size of leaky tumor vasculature.

In this work, we develop theoretical, numerical, and experimental frameworks to apply dynamic magnetic fields to the concentration and deagglomeration of MNPs. Dynamic magnetic fields are characterized by time-dependent changes in the applied magnetic field magnitude, the magnetic field direction, or the magnetic gradient. Here we focus on systems that manipulate the field direction while maintaining quasi-static field gradients such that we can tune interparticle

Received: May 5, 2015

Revised: June 18, 2015

interactions while always promoting local concentration (magnetic targeting). We have added the effect of Brownian motion to our dynamic model to more accurately describe particle suspensions. As proof of principle, Teflon membranes with pore sizes consistent with that found in tumor tissue are fabricated and used as matrices to test the diffusion of MNPs with and without advanced field functions. Disruption of aggregates would enable the MNPs to diffuse more freely through the extracellular matrix while the particles are still driven by the magnetic field gradient (Figure 1). Field functions studied in this work include rotating and other dynamic fields.

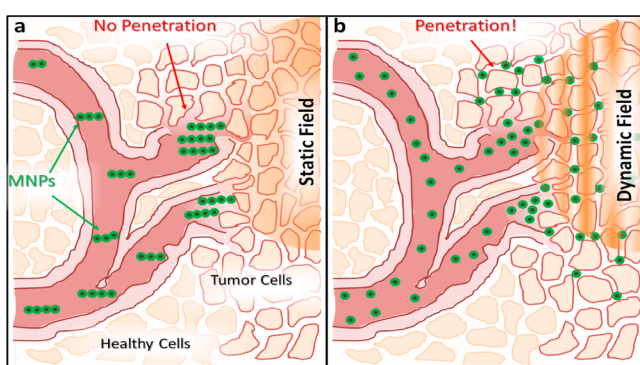


**Figure 1.** Concentration of drug-laden magnetic nanoparticles in tumor sites can be enhanced with dynamic magnetic fields and gradients. (a) Simple magnetic fields and gradients lead to linear aggregation that prevents nanoparticles from entering the pores between tumor cells and densifying within the tumor tissue. (b) Instead, certain dynamic fields similarly concentrate the magnetic nanoparticles at target sites while altogether avoiding aggregation of nanoparticles, thus maximizing the efficiency and effectiveness of drug delivery.

## THEORY

Dipolar interaction between magnetic particles in a static magnetic field leads to formation of chains parallel to the external field. The continuously changing energy landscape of dynamic magnetic fields, on the other hand, prevents magnetic particles from reaching an equilibrium state of aggregation. These dynamics are dictated by viscous drags that need to be taken into account. In general, there exist two regimes: (1) the phase-locked regime, where the orientation between adjacent particles remains fixed relative to the coordinate axis of the changing external field; and (2) the phase-slip regime, where the orientation between adjacent particles can no longer keep up with the changing external field and the particles are, therefore, forced to cycle between attractive and repulsive configurations. These repulsive configurations represent separation events where magnetic particles are driven apart from each other. Here, we have developed a joint analytic (simple Stokes dynamics) and numeric (Langevin-based) description of the response of magnetic particles to dynamic magnetic fields.

**Analytic Theory.** To better understand these systems, we first characterize a symmetric rotating magnetic field in two dimensions. In a symmetric rotating magnetic field, the magnetic particles feel a dipolar force from one another that is based upon their own magnetic moment,  $m$ , and their orientation phase lag,  $\phi_{\text{LAG}}$ , according to either of the following equivalent equations (see Figure 2):

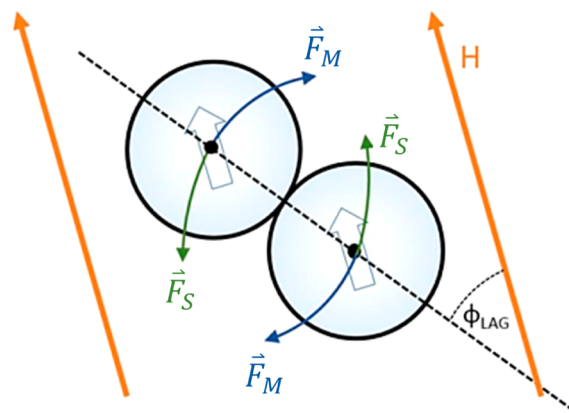


**Figure 2.** Schematic of two aggregated magnetic particles in a rotating magnetic field.

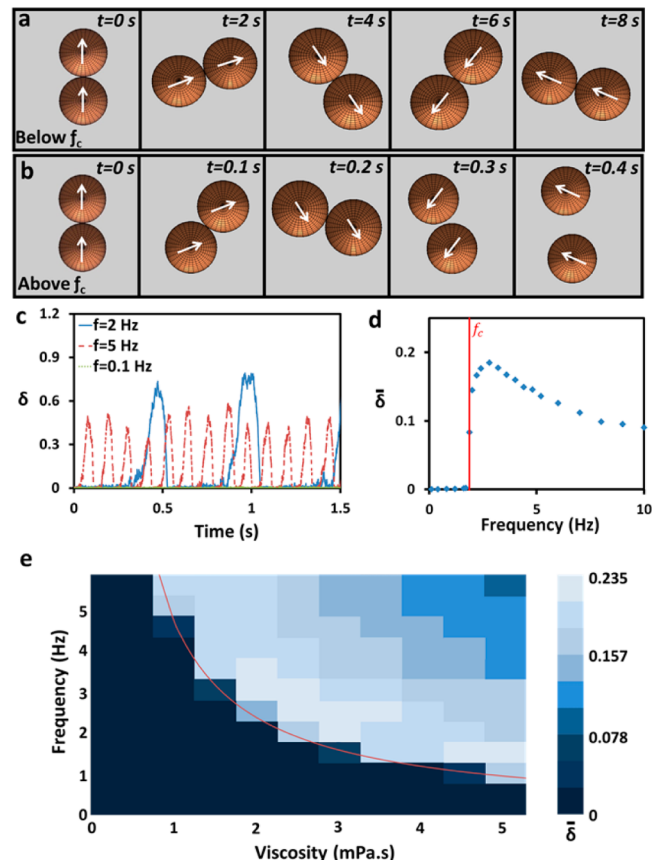


**Figure 3.** Simulation results for  $2a = 2.29 \mu\text{m}$ ,  $\chi = 0.163$ ,  $\eta = 2.5 \text{ mPa s}$  for (a) 0.1 and (b) 2 Hz ( $f_c = 1.87 \text{ Hz}$ ). (c) Normalized separations,  $\delta$ , are plotted over time for different rotational frequencies. (d) There is a nonlinear response in the average separation  $\bar{\delta}$  for a specific viscosity of  $2.5 \text{ mPa s}$ . (e) A phase diagram can be attained for the average de-aggregation separation between two particles across rotational frequencies and viscosities. This compares well with eq 4 (red line).

$$\vec{F}_M = \frac{3\mu_0}{4\pi r^5} \left[ 2(\vec{m} \cdot \vec{r})\vec{m} + (\vec{m} \cdot \vec{m})\vec{r} - \frac{5(\vec{m} \cdot \vec{r})^2}{r^2}\vec{r} \right] \quad (1a)$$

$$\vec{F}_M = \frac{3\mu_0 m^2}{4\pi r^4} [(3 \cos^2 \phi_{\text{LAG}} - 1)\hat{r} + \sin(2\phi_{\text{LAG}})\hat{\theta}] \quad (1b)$$

Here,  $r$  is the center-to-center distance between the particles and  $\mu_0$  is the magnetic constant. The magnetic moment is

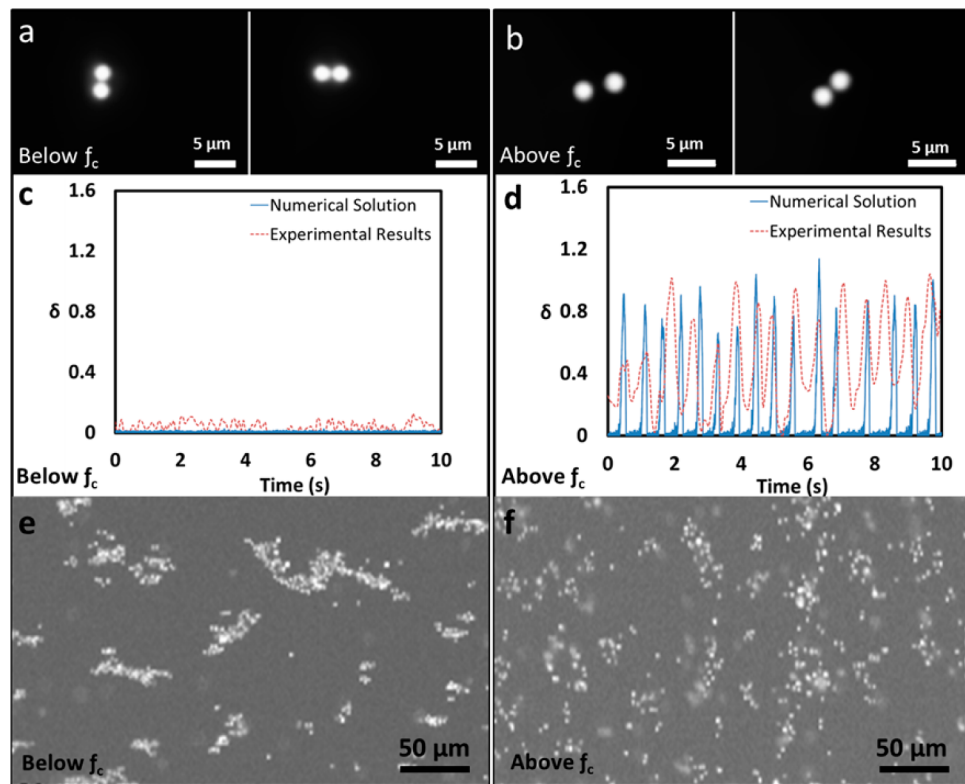


**Figure 4.** Aggregated pairs of  $2.29\text{ }\mu\text{m}$  particles subjected to 100 Oe rotating magnetic fields at (a) 0.1 and (b) 2 Hz. (c) Below the critical frequency for this system ( $f_c = 1.87\text{ Hz}$ ), the particles remain in an aggregated state. (d) Above the critical frequency, many separation events are observed. Numerical simulations agree well with experimental results. (e, f) These observations remain consistent even for higher volume fractions of particle suspensions.

calculated with the linear paramagnetic magnetization formula in SI as  $\vec{m} = 4\pi\chi a^3 \vec{H}/3$  with units of [ $\text{A m}^2$ ] which assumes a low applied field,  $H$ , relative to the magnetic saturation of the particles,  $M_{\text{sat}}$  ( $H \ll M_{\text{sat}}/\chi$ ). Here,  $a$  is the radius of the particles and the susceptibility  $\chi$  is measured for the spherical magnetic particle under consideration and thus takes into account geometric factors such as shape demagnetization factors, permanent clusterings of nanoparticles, and material heterogeneities including polymer coatings. Considering the two equivalent equations, eq 1a can be used in Cartesian coordinates for convenience with our numerical analysis while eq 1b is convenient for our subsequent analytic analysis. We admit that treating the magnetic particles as simple dipoles represents a simplification in this system. As the separation between two particles approaches contact, full multipole expansions of the fields will provide maximum accuracy. Such accuracy is required when attempting to model particles with high susceptibilities or in strong fields. Here, we are well below these thresholds and therefore proceed with simple dipole approximations.

The dipolar force works to keep the magnetic particles chained in line with the instantaneous applied field. As the field precesses, the dipole forces work to rotate the chain so that particles remain phase-locked. The motion of the particles, however, generates a drag force similar to a Stokes force on a particle in flow. The well-known Stokes equation represents the drag force that an isolated particle experiences while it moves through a fluid of viscosity,  $\eta$ , at a velocity,  $v$  as

$$\vec{F}_S = -6\pi\eta a \vec{v}(x, y) \quad (2)$$

A key assumption of Stokes' law is that there are no nearby particles to affect the fluid flow pattern, which would not be true

for the situations considered here. Nonetheless, we employ the Stokes drag expression to describe the hydrodynamics in this system as it enables the use of analytic expressions and later find that experimental results are well-described with this simplification. Two chained particles in line with the applied field experience zero angular force. As the field begins to rotate at a radial frequency of  $2\pi f$ , the angular magnetic force grows with a growing  $\phi_{\text{LAG}}$  until the angular magnetic force balances with the counteracting Stokes force. Here, the velocity of the particles ( $v \sim 2\pi f a$ ) is used in eq 2 to calculate the Stokes force and provides a calculation for the  $\phi_{\text{LAG}}$  required for the particles to stay in the phase-locked condition ( $\phi_{\text{LAG}} = \text{constant}$  and  $r = 2a$ ) as phase-locked regime:

$$\phi_{\text{LAG}} = \frac{1}{2} \sin^{-1}[144\pi\eta f / \mu_0 \chi^2 H^2] \quad (3)$$

There are no solutions for eq 3 when  $144\pi\eta f / \mu_0 \chi^2 H^2 > 1$ , and this condition represents the bifurcation for when the system is driven into the phase-slip regime. Thus, the boundary between these two regimes exists at a critical frequency,  $f_c$ , as follows:

$$f_c = \mu_0 \chi^2 H^2 / 144\pi\eta \quad (4)$$

The angular magnetic force experiences a maximum when  $\phi_{\text{LAG}} = \pi/4$ . If the phase lag gets driven beyond this point (i.e.,  $f > f_c$ ), the two particles will continue to phase slip since the angular magnetic force begins to reduce. Once the particles slip beyond the first magic angle ( $\phi_{\text{LAG}} \approx 0.3\pi$ ), the particles enter a repulsive configuration and the particles are driven to disassemble—have a separation event. As the particles separate, the phase lag continues to slip until it breaches the second magic angle ( $\phi_{\text{LAG}} \approx 0.7\pi$ ), and the particles again have moved into an attractive configuration and reassemble. We believe that such

separation events can be exploited to allow magnetic particles to penetrate porous media during magnetic targeting. It is interesting to note that  $f_c$  is not a function of the particle radius,  $a$ . The accuracy of this expression is therefore questionable when Brownian motion starts to play a significant role in the particle dynamics. Smaller particles will be subjected to higher random forces that would eventually work to drive them apart when they are rotating under fields slightly below the critical frequency. Thus, these smaller particles should experience a higher average separation relative to their radii as compared to larger particles.

Incorporating the Brownian effects of smaller particles can be accomplished with repeated and averaged numerical predictions (Monte Carlo analysis). Along these lines, we also include in this work an effective Brownian force because we are considering the aggregation and breakup of magnetic nanoparticles. Brownian force is randomized according to a white-noise Gaussian function  $\xi$  with a standard deviation of 1 based upon the Einstein diffusion relationship as

$$\vec{F}_{\text{Br}} = k_B T \sqrt{2/\Delta t D} \langle \xi_x \hat{x}, \xi_y \hat{y} \rangle \quad (5)$$

Here,  $k_B$  is Boltzmann's constant,  $T$  is the temperature,  $\Delta t$  is the time step under consideration, and  $D$  is the diffusion coefficient of the particle. We use the Einstein relation  $D = k_B T / 6\pi\eta a$  for the diffusion coefficient which again is in reference to an isolated particle. This effective stochastic Brownian force ( $T = 298$  K) is included in all of the numerical simulations in this work.

**Numerical Simulations.** To complement the obtained analytic expression, a numerical simulation has been developed to observe separation events between particles at different frequencies (below, above, and at  $f_c$ ) using particle simulation dynamics modeled with a Matlab code. The force balance was used to determine the instantaneous velocity of the particles at each time step of the simulation according to the following Langevin equation:

$$\vec{F}_{\text{NET}} = \tilde{m} \frac{d\vec{v}}{dt} = \vec{F}_M + \vec{F}_S + \vec{F}_{\text{Br}} \quad (6)$$

For microparticle simulations, the inertial term can be neglected allowing eqs 1a, 2, 5, and 6 to be combined to solve for the instantaneous particle velocity,  $v$ . A simulation run involves calculating the new position of a particle at each time step according to

$$P(x, y, t) = P(x, y, t - \Delta t) + \vec{v}(x, y)\Delta t \quad (7)$$

Here,  $P$  represents the position of the particle in space as a function of time,  $t$ . In simulations of microparticles ( $2a = 2.29 \mu\text{m}$ ), the time step,  $\Delta t$ , was taken to be 0.1 ms to minimize run time. We consider the particles to be hard spheres in the simulation by not allowing overlapping configurations to occur (see the SI for more details).

## MATERIALS AND METHODS

**Magnetic Particles.** Two different synthesized and commercial magnetic micro- and nanoparticles were employed in this study including  $2.29 \mu\text{m}$  fluorescent magnetic polystyrene particles (Microspheres-Nanospheres, Corpucular,  $\chi = 0.163$ ), and  $150 \text{ nm}$  PEG-coated iron oxide nanoparticles (synthesized,  $\chi = 4.36$ ). The microparticles were used to validate our numerical theory, test our hypotheses, and relax the cost of our numerical simulations. The sizing of the  $2.29 \mu\text{m}$  particles was verified with scanning electron microscopy. The magnetic susceptibilities indicated earlier were determined using a MPMS-XL superconducting quantum interference device magnetometer (Quantum

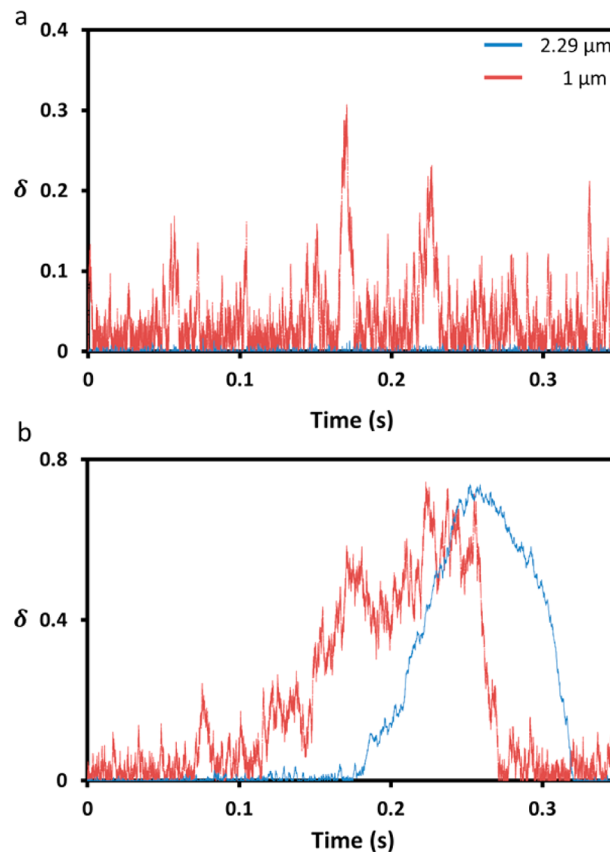


**Figure 5.** Simulation results for 1 and  $2.29 \mu\text{m}$  particles at (a) 0.1 and (b) 2.5 Hz ( $\chi = 0.163$ ;  $\eta = 2.5 \text{ mPa s}$ ). Increased Brownian motion is observed for 1  $\mu\text{m}$  particles.

Design Inc., San Diego, CA, USA). The particles were initially in aqueous suspensions and were added volumetrically to glycerol–water solutions for in situ testing. The 150 nm particles were synthesized according to literature.<sup>17</sup> Briefly, fluidMAG-D starch-coated iron oxide nanoparticles (chemicell GmbH, Germany) were cross-linked with epichlorohydrin and then reacted with ammonium hydroxide to produce an aminated magnetic nanoparticle (MNP). The aminated MNP was then reacted with methoxyl polyethylene glycol succinimidyl ester (mPEG-NHS) to obtain the PEGylated magnetic nanoparticles. Analysis of the particles using a Zetasizer Nano ZS (Malvern, Worcestershire, U.K.) dynamic light scattering instrument yielded an average intensity-based hydrodynamic diameter of  $144 \pm 18 \text{ nm}$  and a zeta potential of  $37.4 \pm 1.7 \text{ mV}$ .

**Magnetic Field Setup.** Magnetic fields were applied either with computer-controlled solenoids (low gradient) or a motorized permanent magnet (high gradient). For the case of the low-gradient field, two 4 in. diameter iron-core solenoids are positioned in the  $x$  direction and the  $y$  direction. The solenoids are fed with current from two 20-5M bipolar operational amplifiers (Kepco) controlled with a LabView program. For the high-gradient system, a motorized 2 in. by 2 in. square rare-earth magnet magnetized through the 0.5 in. thickness (K&J Magnetics) was used. During field application, particles were observed using a customized column-mounted microscope (Nikon). Visualization of 150 nm particles was made possible by using a dark-field attachment (MVI Darklite).

**In Situ Penetration Studies.** For this study, a capillary system was designed that exhibited a scaffold barrier in the middle of the capillary (Figure 7a). The capillary was constructed from polypropylene tubing sealed with epoxy to contain Teflon scaffolding that has 2  $\mu\text{m}$  pores. The Teflon scaffolding was removed from a PTFE filter (Catalog No. SF200T, Environmental Express). A 10  $\mu\text{L}$  aliquot of MNPs suspension with a concentration of  $1.12 \text{ mg/mL}$  was injected in the input port of the capillary system while applying either dynamic or static magnetic fields. After 1 h, the output port was entirely collected to analyze the amount

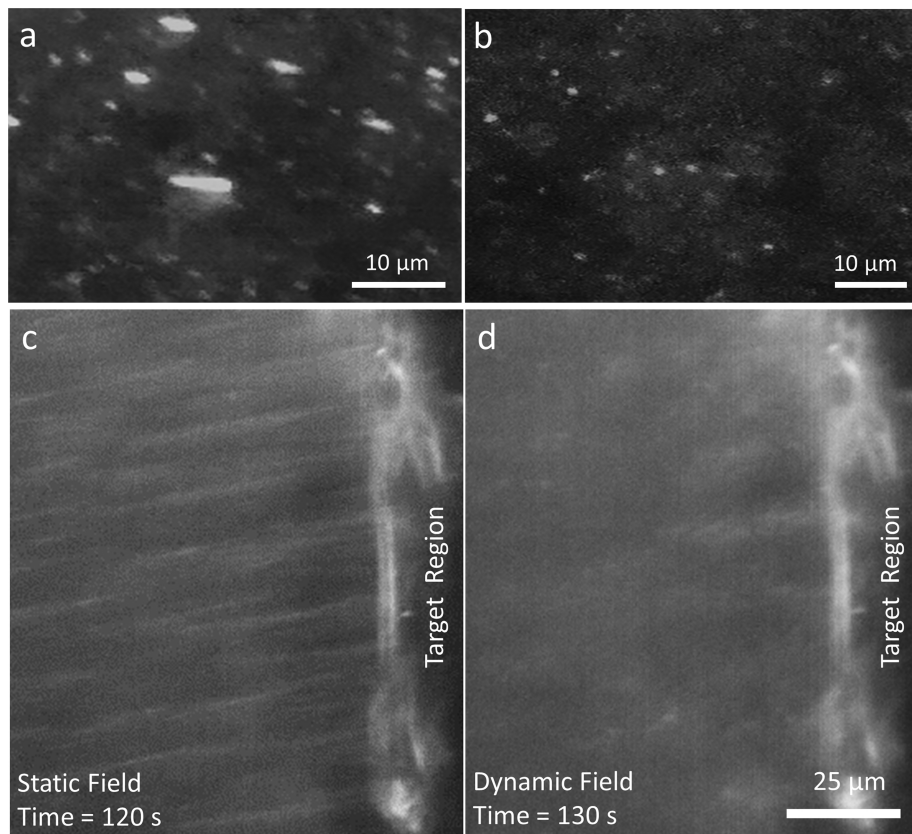


**Figure 6.** Experimental dark-field micrographs of 150 nm magnetic particles under rotating fields of (a) 0.1 and (b) 2.5 Hz frequency. (c) Significant aggregation in 150 nm magnetic nanoparticles under static fields after 2 min. The magnetic field gradient was 60 Oe/cm, and the applied magnetic field was 165 Oe. (d) Dynamic fields studied here immediately de-aggregate nanoparticles while maintaining 165 and 60 Oe/cm.

of penetrated MNPs. Analysis of penetration was conducted with intensity measurements (measured with image analysis using ImageJ). An exponential relation between intensity and concentration was found based on solutions with known concentrations, and then by using this relation, the concentration of each sample was calculated (see the SI for more details).

## RESULTS AND DISCUSSION

### Rotating Magnetic Fields with Constant Gradient.

Simple rotating fields with gradients were first considered for simultaneously concentrating and de-aggregating magnetic particles. To understand magnetic particle responses to rotating fields, numerical predictions were conducted using the approach detailed in Numerical Simulations. In each case a range of frequencies was tested and the simulation results were analyzed.

An example of simulation results for two 2.29  $\mu\text{m}$  particle assemblies above and below the critical frequency calculated according to eq 4 is shown in Figure 3a,b for a fluidic environment of  $\eta = 2.5 \text{ mPa s}$ . Below the critical frequency, the angular magnetic forces work to rotate the chains with the rotating field but are counteracted by the viscous forces working against this reorientation. This force balance develops the expected phase lag predicted by eq 3 (see the SI).

As the rotational frequency of the applied field is increased beyond the critical frequency, the viscous forces drive the particles into the phase-slip regime. Once the particles rotate beyond the magic angle, the interaction of their moments induces repulsive interactions, creating a separation ( $\Delta$ ). Tracking of the separation between these simulated particles normalized to the particle radius,  $\delta = \Delta/a$ , is shown in Figure 3c

for frequencies below  $f_c$  (0.1 Hz), near  $f_c$  (2 Hz), and well above  $f_c$  (5 Hz). The average separation,  $\bar{\delta}$ , was tracked for a range of frequencies and is shown in Figure 3d, demonstrating the nonlinear dynamics of the response to the oscillating field by this particle pair. At higher frequencies, separation events are more frequent but less significant. At the critical frequency, separation events are the largest but occur less frequently. Thus, maximum separation of the magnetic particles occurs in the region slightly above the critical frequency, where the separation events are both significant and somewhat frequent. This realization highlights the importance of properly characterizing the experimental system in each case to maximize de-aggregation.

These simulations were carried out across the design space of frequency and viscosity to compare the numerically observed critical frequency with the analytic value derived from eq 4. As shown in Figure 3e, the analytic theory (red line) and the numerical prediction are determined to nicely agree with each other.

The numerical simulation and the analytic model were then compared against experimental observations of several different two particle assemblies in a  $\eta = 2.5 \text{ mPa s}$  carrier fluid. Figure 4 shows 2.29  $\mu\text{m}$  particles oscillating in a rotating magnetic field. Below the critical frequency ( $f = 0.1 \text{ Hz}$ , Figure 4a), the two particles are able to stay aggregated and rotate with the applied field. Above the critical frequency ( $f_c = 1.87 \text{ Hz}$ , Figure 4b), separation events were observed during field application. The separation  $\delta$  between the two particles was tracked in both cases and closely matched the numerical predictions that incorporate Brownian motion (Figure 4c,d).

To investigate the scalability of these phenomena to suspensions of magnetic particles that have high solid loadings,

rotating fields both above and below the critical frequency were applied to 1 vol % of  $2.29\text{ }\mu\text{m}$  particles suspended in a carrier fluid of viscosity  $\eta = 2.5\text{ mPa s}$ . Below the critical frequency ( $f = 0.1\text{ Hz}$ , Figure 4e), the magnetic particles strongly aggregated with the field rotating slowly. Above the critical frequency ( $f = 2\text{ Hz}$ , Figure 4f), the magnetic particles completely de-aggregated. In both cases, a strong magnetic field gradient can be applied to concentrate these particles in a target region such as for drug delivery. These systems were investigated at higher viscosities, and similar agreement with eq 4 was found (see the SI).

Again, these simulation and experimental results include the effect of random Brownian motion that lead to the small deviations between cycles of the applied external field. For these  $2.29\text{ }\mu\text{m}$  particles, Brownian motion has a relatively small effect (the slight variations in the numerical simulation plots). However, many particles of interest for magnetic targeting and drug delivery are typically in the nanometer range where Brownian motion plays a more disrupting role. Figure 5 compares the simulated behavior of 1 and  $2.29\text{ }\mu\text{m}$  microparticles with relatively low susceptibilities ( $\chi = 0.163$ ). For these lower susceptibilities, the randomizing Brownian forces have contributions toward dominating the confining magnetic interparticle forces. In general, smaller particles show a higher tendency to de-aggregate, but even nanoparticles of sufficient susceptibility will quickly aggregate and form significant chains under applied fields (Figure 6).

Though de-aggregation in these systems is aided by Brownian motion, nanoparticles of sufficient size and magnetic susceptibility still form linear chains in experiments under modest applied fields (100 Oe). Experiments were completed with synthesized  $150\text{ nm}$  magnetic particles exhibiting magnetic susceptibility of  $\chi = 4.36$ . In these nanoparticle suspensions, linear aggregation of  $150\text{ nm}$  magnetic nanoparticles occurs very quickly in 100 Oe magnetic fields (Figure 6c, Supporting Information Video 1). Under rotating fields of low frequencies,  $150\text{ nm}$  magnetic particles will still form chains despite the influence of Brownian motion (Supporting Information Figure S4). These chains can easily reach lengths of  $3\text{ }\mu\text{m}$  within short times which is, for example, above the characteristic porosity of tumor tissue. This observation establishes the significance of running these field setups at higher frequencies to allow for the proper de-aggregation of the magnetic particles. At higher frequencies of  $2.5\text{ Hz}$ , the magnetic nanoparticles were found to de-aggregate below the visible length scale of the dark-field microscope setup (Figure 6b). This frequency is still well below the critical frequency (for these strongly magnetic particles at  $\chi = 4.36$ ). Therefore, based on our microparticle investigations, we believe that though complete de-aggregation down to individual nanoparticles is not occurring, the longer particle chains are indeed being broken apart. For most delivery applications, maintaining aggregate sizes below  $500\text{ nm}$  is sufficient to penetrate porous tissues.

A rotating field was then combined with a magnetic field gradient to locally concentrate the nanoparticles by using the motorized permanent magnet setup. In this system, the permanent magnet attracted the  $150\text{ nm}$  particles to a target area (Figure 6c,d). Clear linear aggregation of the magnetic particles occurred during this step. Then, the magnetic field was rotated slightly above the critical frequency and the chains quickly de-aggregated within seconds. The field rotation was then interrupted and the nanoparticles again quickly re-formed linear aggregates near the target area.

**Applying De-aggregation Field Functions in Situ.** It has been demonstrated that linear aggregation of  $150\text{ nm}$

magnetic particles occurs very quickly under relatively low applied magnetic fields. We expect that if these aggregates grow beyond the characteristic length of a porous network, then the diffusion of the aggregates through that network will become extremely limited. These aggregations can be broken by using advanced field functions for the magnetic field. On the other hand, we expect that if these aggregates are well below the characteristic length of a porous network, they may actually experience faster transport through the network due to enhanced magnetization from neighboring particles in the aggregate. Thus, the ideal choice of dynamic fields assuredly depends on the size of the porous network. To better characterize the system, dynamic and static magnetic fields of equal strength and field gradient (480 and  $430\text{ Oe/cm}$ ) were applied to magnetic nanoparticle suspensions carefully injected to the leading edge of a porous network made out of Teflon fiber mesh characterized by a pore size of  $\sim 2\text{ }\mu\text{m}$  (Figure 7a). Under the case of a dynamic

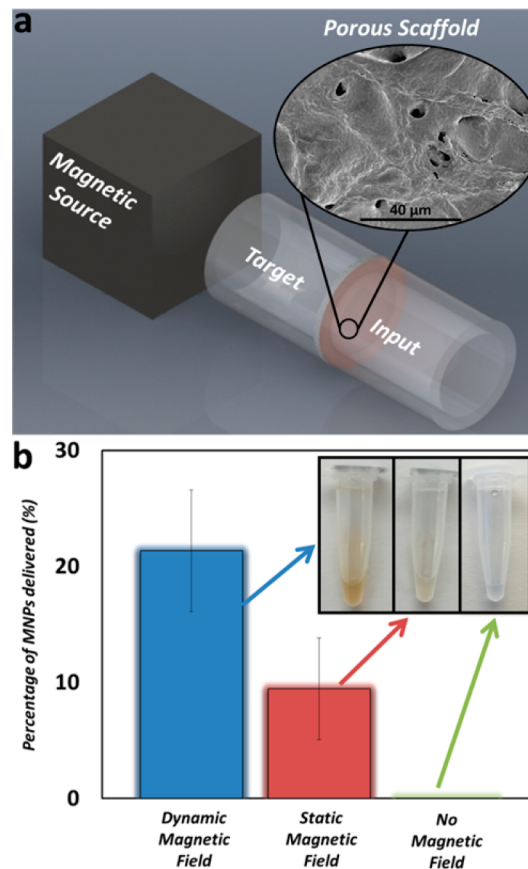


**Figure 7.** (a) Schematics of the in situ setup. (b) Percentage of delivered  $150\text{ nm}$  MNPs after applying dynamic and static magnetic field for 1 h.

magnetic field, the penetration of MNPs through the porous scaffold was enhanced by 2-fold. This enhancement is believed to be enabled by the separation events that work to de-aggregate the magnetic nanoparticle chains bringing the effective aggregate size to a length less than the pore size. This result suggests that if static magnetic sources are replaced by dynamic counterparts during magnetic targeting, the treatment will have more efficacy for extravasation of the MNPs out of the vasculature and into the porous cellular tissue.

**Advanced Field Functions.** Though simple rotating field functions are effective in de-aggregating magnetic particles from

each other, more complex field functions have the possibility of enhancing  $\delta$ . Higher  $\delta$  is expected to generally coincide with more isolated particles in the concentration zone though this is dependent upon the local packing fraction of the particles.

The design space of 3D advanced field functions is very large. To highlight this, we show a few examples of 2D field functions that lead to higher  $\delta$  than the rotating field function at the critical frequency. First, a stepped function is considered (the red line in Figure 8a) where the field switches directly from 100 Oe in the

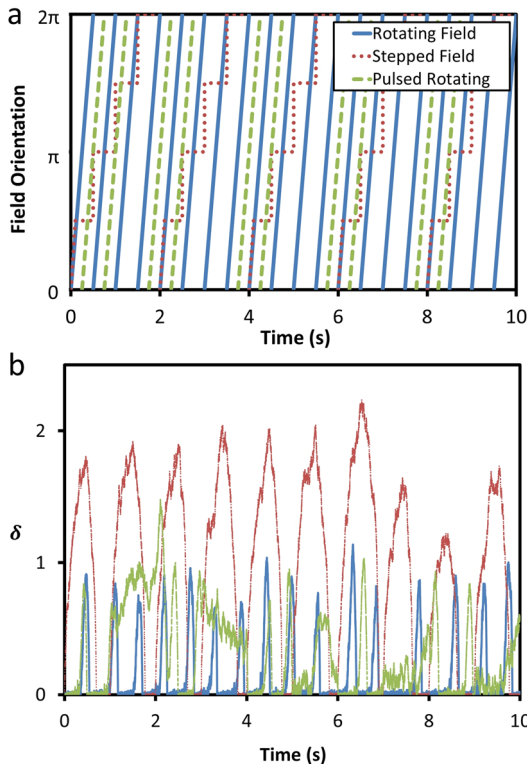


**Figure 8.** (a) Functions that have been used for the field setup. (b) Separation events obtained numerically ( $2a = 2.29 \mu\text{m}$ ;  $\chi = 0.163$ ;  $\eta = 2.5 \text{ mPa s}$ ).

$x$  direction to 100 Oe in the  $y$  direction at a frequency of 2 Hz. Applying this magnetic field to the numerical simulation shows very large de-aggregation (high  $\delta$ ) compared to the standard rotating magnetic field function and also the pulsed rotating field function (Figure 8b).

Similarly, another advanced field function of a pulsed rotating field with a rotational frequency of  $f = 2$  Hz and pulse frequency of 1 Hz was simulated (green line in Figure 8a). This field function gives a relatively higher average separation compared to the rotating field. In this setup the time interval during which field is off should not be large since there is a chance of losing the concentration of the particles. By tuning the applied dynamic fields, particles can stay de-aggregated for significantly longer times compared to the static fields currently used, while concurrently maintaining a strong magnetic field gradient.

## CONCLUSIONS

Here we suggest a method for driving the disassembly of magnetic nanoparticles under dynamic magnetic fields during magnetic targeting. This technique resolves the issues associated with particle aggregation during magnetic targeting implementations. By exploiting dynamic fields, a dynamic energy landscape is

generated that can catch particles in repulsive configurations, causing them to break apart. This disassembly process allows the magnetic nanoparticles to travel into the smallest capillaries such as the extracellular channels between tumor cells. In situ experiments that recreate porous tissue with a Teflon scaffolding show that penetration of the MNPs is enhanced by 2-fold with dynamic magnetic fields compared to static fields. This result suggests that dynamic fields could indeed provide a large enhancement to the efficiency of magnetic targeting schemes by allowing the MNPs to permeate extensively into porous tissues.

## ASSOCIATED CONTENT

### Supporting Information

Supplementary videos, text discussing numerical simulation, calibration curve for intensity/concentration measurements, and viscosity dependence, table listing the differential particle types tested, and figures showing phase lag as a function of applied frequency, maximum normalized separation and frequency of separation events, intensity vs concentration curve, and response of magnetic particles suspensions. The Supporting Information is available free of charge on the ACS Publications website at DOI: 10.1021/acs.langmuir.5b01458.

## AUTHOR INFORMATION

### Corresponding Author

\*E-mail: r.erb@neu.edu.

### Notes

The authors declare no competing financial interest.

## ACKNOWLEDGMENTS

This material is based in part upon work supported by the National Science Foundation under Grant Number CPS-1329649.

## REFERENCES

- Jemal, A.; Siegel, R.; Xu, J.; Ward, E. *Cancer Statistics 2010*. *Cancer J. Clin.* **2010**, *60*, 277–300.
- Rooseboom, M.; Commandeur, J. N. M.; Vermeulen, N. P. E. Enzyme-Catalyzed Activation of Anticancer Prodrugs. *Pharmacol. Rev.* **2004**, *56*, 53–102.
- Elias, A.; Crayton, S. H.; Warden-Rothman, R.; Tsourkas, A. Quantitative Comparison of Tumor Delivery for Multiple Targeted Nanoparticles Simultaneously by Multiplex ICP-MS. *Sci. Rep.* **2014**, *4*, 5840–9.
- Kirpotin, D. B.; Drummond, D. C.; Shao, Y.; Shalaby, M. R.; Hong, K.; Nielsen, U. B.; Marks, J. D.; Benz, C. C.; Park, J. W. Antibody Targeting of Long-Circulating Lipidic Nanoparticles Does Not Increase Tumor Localization but Does Increase Internalization in Animal Models. *Cancer Res.* **2006**, *66*, 6732–6740.
- Zhou, J.; Zhang, J.; David, A. E.; Yang, V. C. Magnetic tumor targeting of  $\beta$ -glucosidase immobilized iron oxide nanoparticles. *Nanotechnology* **2013**, *24*, 375102-1–375102-12.
- David, A. E.; Cole, A. J.; Chertok, B.; Park, Y. S.; Yang, V. C. A combined theoretical and in vitro modeling approach for predicting the magnetic capture and retention of magnetic nanoparticles in vivo. *J. Controlled Release* **2011**, *152*, 67–75.
- Yuan, F.; Dellian, M.; Fukumura, D.; Leunig, M.; Berk, D. A.; Torchilin, V. P.; Jain, R. K. Vascular Permeability in a Human Tumor Xenograft: Molecular Size Dependence and Cutoff Size. *Cancer Res.* **1995**, *55*, 3752–3756.
- Wang, J.; Lu, Z.; Gao, Y.; Wientjes, M. G.; Au, J. L. S. Improving delivery and efficacy of nanomedicines in solid tumors: role of tumor priming. *Nanomedicine* **2011**, *6*, 1605–1620.

- (9) Biswal, S. L.; Gast, A. P. Rotational dynamics of semiflexible paramagnetic particle chains. *Phys. Rev. E* **2004**, *69*, 041406-1–041406-9.
- (10) Vuppu, A. K.; Garcia, A. A.; Hayes, M. A. Video Microscopy of Dynamically Aggregated Paramagnetic Particle Chains in an Applied Rotating Magnetic Field. *Langmuir* **2003**, *19*, 8646–8653.
- (11) Biswal, S. L.; Gast, A. P. Mechanics of semiflexible chains formed by poly(ethylene glycol)-linked paramagnetic particles. *Phys. Rev. E: Stat. Phys., Plasmas, Fluids, Relat. Interdiscip. Top.* **2003**, *68*, 021402-1–021402-9.
- (12) Biswal, S. L.; Gast, A. P. Micromixing with Linked Chains of Paramagnetic Particles. *Anal. Chem.* **2004**, *76*, 6448–6455.
- (13) Melle, S.; Calderón, O. G.; Rubio, M. A.; Fuller, G. G. Microstructure evolution in magnetorheological suspensions governed by Mason number. *Phys. Rev. E: Stat. Phys., Plasmas, Fluids, Relat. Interdiscip. Top.* **2003**, *68*, 041503-1–041503-11.
- (14) Kang, T. G.; Hulsen, M. A.; Anderson, P. D.; den Toonder, J. M. J.; Meijer, H. E. H. Chaotic mixing induced by a magnetic chain in a rotating magnetic field. *Phys. Rev. E* **2007**, *76*, 066303-1–066303-11.
- (15) Sandre, O.; Browaeys, J.; Perzynski, R.; Bacri, J. C.; Cabuil, V.; Rosensweig, R. E. Assembly of microscopic highly magnetic droplets: Magnetic alignment versus viscous drag. *Phys. Rev. E: Stat. Phys., Plasmas, Fluids, Relat. Interdiscip. Top.* **1999**, *59*, 1736–1746.
- (16) Melle, S.; Fuller, G. G.; Rubio, M. A. Structure and dynamics of magnetorheological fluids in rotating magnetic fields. *Phys. Rev. E: Stat. Phys., Plasmas, Fluids, Relat. Interdiscip. Top.* **2000**, *61*, 4111–4117.
- (17) Cole, A. J.; David, A. E.; Wang, J.; Galbán, C. J.; Hill, H. L.; Yang, V. C. Polyethylene glycol modified, cross-linked starch-coated iron oxide nanoparticles for enhanced magnetic tumor targeting. *Biomaterials* **2011**, *32*, 2183–2193.